

Wavelet bispectral analysis for the study of interactions among oscillators whose basic frequencies are significantly time variable

Janez Jamšek,^{1,2,3} Aneta Stefanovska,^{1,3} and Peter V. E. McClintock³

¹*Group of Nonlinear Dynamics and Synergetics, Faculty of Electrical Engineering, University of Ljubljana, Tržaška 25, 1000 Ljubljana, Slovenia*

²*Department of Physics and Technical Studies, Faculty of Education, University of Ljubljana, Kardeljeva ploščad 16, 1000 Ljubljana, Slovenia*

³*Department of Physics, University of Lancaster, Lancaster LA1 4YB, United Kingdom*

(Received 24 April 2007; published 24 October 2007)

Bispectral analysis, recently introduced as a technique for revealing time-phase relationships, is extended to make use of wavelets rather than Fourier analysis. It is thus able to encompass instantaneous phase-time dependence for the case of two or more coupled nonlinear oscillators. The method is demonstrated and evaluated by use of test signals from a pair of coupled Poincaré oscillators. It promises to be useful in a wide range of scientific contexts for studies of interacting oscillators whose basic frequencies are significantly time variable.

DOI: [10.1103/PhysRevE.76.046221](https://doi.org/10.1103/PhysRevE.76.046221)

PACS number(s): 05.45.Xt, 05.45.Tp, 02.70.Hm

I. INTRODUCTION

Coupled oscillatory systems are found in a diversity of different contexts in science and technology, including, e.g., engineering structures such as bridges [1,2], the flashing of male fireflies [3], the mammalian cardiorespiratory system [4,5], the physics of plasmas [6], laser arrays [7], and chaos [8]. Their understanding requires a knowledge of the interoscillator interactions, and a common problem lies in extracting this information from measurements of oscillator coordinates, usually recorded in the form of time series. Where bivariate data are available for a pair of interacting oscillators (i.e., where the coordinate of each of them can be measured separately), phase relationships can be obtained by use of the methods recently developed for analysis of synchronization, or generalized synchronization, between chaotic and/or noisy systems. Not only can the interactions be detected [9], but their strength and direction can also be determined [10]. The next logical step in studying the interoscillator interactions from measured data was to determine the type of the couplings [11], as the methods developed for synchronization analysis are not capable of answering this question.

Systems are usually taken to be stationary. In reality, however, mutual interactions among their subsystems often result in time variability of the characteristic frequencies. Frequency and phase couplings sometimes occur only transiently, and the strength of coupling between pairs of individual oscillators may change with time. Under these circumstances, conventional bispectral analysis for stationary signals, based on time averages, is no longer sufficient. Rather, the time evolution of the bispectral estimates is needed. Priestley and Gabr [12] were probably the first to introduce the time-dependent bispectrum for harmonic oscillators. Most subsequent work has been related to the time-frequency representation and is based on high-order cumulants [13]. An extensive overview can be found in [14].

Schack *et al.* [15] have recently introduced a time-varying spectral method for estimating the bispectrum and bicoher-

ence: they obtain estimates by filtering in the frequency domain and then obtaining a complex time-frequency signal by inverse Fourier transform. They assume, however, that the interacting oscillators are harmonic. Millingen *et al.* [16] introduced the wavelet bicoherence and were the first to demonstrate the use of bispectra for studying interactions among nonlinear oscillators. They used the method to detect periodic and chaotic interactions between two coupled van der Pol oscillators, but without concentrating on time-phase relationships in particular.

In an earlier paper [11], we extended bispectral analysis to encompass time dependence, and demonstrated the potential of the enhanced technique to determine the types of coupling among interacting nonlinear oscillators. Time-phase couplings can be observed by calculating the bispectrum and adapted bispectrum, thereby obtaining the time-dependent biphasic and biamplitude. This method has the advantage that it allows an arbitrary number of interacting oscillatory processes to be studied. It is applicable both to univariate (a single signal from the coupled system), and to multivariate data (a separate signal from each oscillator). It yields results that are applicable quite generally to any system of coupled nonlinear oscillators.

In the present paper, we introduce a new technique likely to be useful for studying complex oscillatory systems whose characteristic frequencies vary in time, e.g., the human cardiovascular system [5]. It is able to reveal both the existence of interactions among the subsystems, and also the nature of the interactions. Cardiovascular signals are highly complex from the nonlinear dynamics point of view. Their frequencies and amplitudes, and the couplings among the subsystems, are all time variable. To be able to cope with this type of signal we have incorporated wavelets into the technique and further extended it for studying the instantaneous phase couplings.

In what follows, however, we are mainly concerned with basic principles, and in demonstrating and testing the technique on a well-characterized simple model. Application to the more challenging problems posed by, e.g., the cardiovas-

cular system itself, currently in progress, will be described elsewhere.

In Sec. II we introduce the technique and in Sec. III we describe how it has been tested on a model coupled-oscillator system. The relative advantages and disadvantages of the Fourier and wavelet bispectral methods are discussed in Sec. IV. Finally, in Sec. V we summarize the results obtained and draw conclusions.

II. METHOD

A. Time-phase bispectral analysis

We start by summarizing briefly the salient features of time-phase bispectral analysis as based on the Fourier transform. For a detailed discussion, see [11].

The classical bispectrum estimate is obtained as an average of estimated third-order moments (cumulants) $\hat{M}_3^i(k, l)$ [17],

$$\hat{B}(k, l) = \frac{1}{K} \sum_{i=1}^K \hat{M}_3^i(k, l), \quad (1)$$

where the third-order moment estimate $\hat{M}_3^i(k, l)$ is performed by a triple product of discrete Fourier transforms (DFTs) at discrete frequencies k , l , and $k+l$,

$$\hat{M}_3^i(k, l) = X_i(k)X_i(l)X_i^*(k+l). \quad (2)$$

Here $i=1, \dots, K$ label the time segments into which the signal has been divided. The bispectrum $B(k, l)$ is a complex quantity, defined by magnitude A and phase ϕ ,

$$B(k, l) = |B(k, l)|e^{j\angle B(k, l)} = Ae^{j\phi}. \quad (3)$$

For each (k, l) , the value of $B(k, l)$ can be represented as a point in the space, $\text{Re}[B(k, l)]$ versus $\text{Im}[B(k, l)]$, thus defining a vector whose magnitude (length) is known as the bi-amplitude. The phase is determined by the angle between this vector and the positive real axis and for the bispectrum is called the biphase.

To encompass time dependence within bispectral analysis in analogy with the short-time Fourier transform, we can move a time window $w(n)$ of length M across the signal $x(n)$ and calculate the discrete Fourier transform at each window position,

$$X(n, k) \cong \frac{1}{M} \sum_{i=0}^{M-1} x(i)w(i-n)e^{-j2\pi ik/M}, \quad (4)$$

where k is the discrete frequency and n the discrete time. The instantaneous biphase calculated from Eqs. (1) and (3) is then

$$\phi(k, l, n) = \phi_k(n) + \phi_l(n) - \phi_{k+l}(n). \quad (5)$$

Simultaneously, we observe the instantaneous bi-amplitude, from which it is possible to infer the relative strength of the interaction. It is thus possible to detect and quantify the presence of coupling among the oscillators and to follow its persistence in time.

B. Wavelet bispectrum

The Fourier transform is based on the presumptions of (a) periodicity and (b) infinite length of the signal series [18,19]. Because neither assumption can be strictly true for any measured signal, the determination of separate frequencies in a system that possesses strong couplings is very demanding. The difficulty is greater in the low-frequency range, which is of particular interest to us, because the characteristic frequencies are close to each other and are therefore even harder to separate. The uncertainty principle governing the Fourier transform limits its ability to separate harmonic components in the frequency domain of the bispectrum [20,21]. This might cause problems for detection of quadratic phase couplings in the case of frequency pairs that are close together. To ensure good resolution of low frequencies, we need longer sections for calculation of the discrete Fourier transform. This immediately decreases the number of sections possible and weakens the bispectrum estimation. However, we cannot use longer signals, because they lead to non-stationarity, and the variance consequently becomes even larger [22]. One way of accommodating these conflicting demands is through the introduction of wavelet analysis.

Wavelet analysis can be seen as a generalization of Fourier analysis [21] by the addition of time resolution—in a more fundamental way than is permitted by the short-time Fourier transform (STFT) [23]. Wavelet analysis has been applied with considerable success to cardiovascular data [24]. A generalization of bispectral analysis, based on wavelets, may be expected to be able to detect temporal variations in phase coupling, or short-lived couplings, and to cope with broadened and coalescing peaks that cannot be resolved due to the time-frequency resolution restrictions that govern the STFT-based bispectrum.

Wavelet analysis was first introduced by Morlet [25]. It enables the window length to be adjusted to the frequency currently being analyzed. It is a scale-independent method. It uses a window function known as the mother wavelet, or basic wavelet $\psi(u)$, which can be any function that satisfies the wavelet admissibility condition [21]. This function introduces a scale s (its width) into the analyses. Commitment to any particular scale is avoided by using all possible scalings of $\psi(u)$. The mother wavelet is also translated along the signal to achieve time localization. Thus, a family of generally nonorthogonal basis functions is obtained,

$$\Psi(s, t) = |s|^{-p} \psi\left(\frac{u-t}{s}\right). \quad (6)$$

The parameter p is an arbitrary non-negative number, used for normalization. Values of p of 0, 1/2, and 1 are encountered in the literature [26]. The prevailing choice of $p=1/2$ yields a factor $|s|^{-1/2}$ and ensures energy conservation. In this case, the L^2 norm of the wavelet, and thus its energy, is unaffected by the scaling operator s . The continuous wavelet transform $W_g(s, t)$ of a signal $g(t)$ is defined as:

$$W_g(s, t) = \int_{-\infty}^{\infty} \Psi^*\left(\frac{\tau-t}{s}\right)g(\tau)d\tau \quad (7)$$

and is a mapping of the function $g(t)$ onto the time scale plane.

In numerical applications, the scale s and time t are restricted to take discrete values. A natural discretization of the scaling parameter is $s_m = \sigma^m$, where $m \in \mathbb{Z}$, and the step is a positive number $\sigma \neq 0, 1$. Within the scale σ^m , the signal is sampled only at times $t_n = n\sigma^m$, which means that the sampling rate is automatically adjusted to the scale [21].

For different values of m and n , we obtain the discrete wavelet family

$$\Psi_{m,n}(u) = \sigma^{-m/2} \psi(\sigma^{-m}u - n\tau), \quad (8)$$

where we have set $p=1/2$. The discrete wavelet transform, defined by this family, is simply a sampled version of $W_g(s, t)$. By choosing σ near 1, we can obtain a representation close to the continuous transform.

1. Direct relationship between the scale and the frequency using Morlet wavelets

Coupling between wavelets makes sense when a frequency can be assigned to the wavelet. We restrict our attention to wavelets whose Fourier transforms exhibit a single dominant peak, and we define the location of that peak as being the corresponding frequency. In the literature [21], several suitable wavelets are mentioned. Following earlier energy density studies of measured cardiovascular signals, the Morlet mother wavelet was chosen [24].

Morlet proposed the use of a Gaussian function modulated by a sine wave. Its Fourier transform is a shifted Gaussian, adjusted slightly so that the admissibility condition $\hat{\psi}(0)=0$ is satisfied:

$$\hat{\psi}(f) = \sqrt{2\pi} \frac{1}{\sqrt{4\pi}} (e^{-4\pi^2(f-f_0)^2/2} - e^{4\pi^2 f^2/2} - e^{4\pi^2 f_0^2/2}). \quad (9)$$

The corresponding time domain expression is

$$\psi(u) = \pi^{-1/4} (e^{-j2\pi f_0 u} - e^{4\pi^2 f_0^2/2}) e^{-u^2/2}. \quad (10)$$

The choice of f_0 represents a compromise between localization in time and in frequency. For smaller f_0 , the shape of the wavelet favors localization of singular time events whereas, for larger f_0 , more periods of the sine wave within the window improve the frequency localization. For $f_0 > 0.8$, the value of the second term in (10) is so small that it can be ignored in practice, and a simplified expression for the Morlet wavelet in the time domain is

$$\psi(u) = \pi^{-1/4} e^{-j2\pi f_0 u} e^{-u^2/2}. \quad (11)$$

The corresponding wavelet family consists of Gaussians centered on a time t and with standard deviation s . In the frequency domain, we have Gaussians with a central frequency $f = f_0/s$ and a standard deviation of $1/2\sqrt{2}\pi s$. Thus, application of the wavelet transform at a given scale s can also be interpreted as bandpass filtering, giving an estimation of the contribution to the frequencies in this band. The relationship between the scale and the central frequency for the Morlet wavelet is then

$$f = \frac{f_0}{s}. \quad (12)$$

The frequency resolution changes with frequency. At low frequencies (large scales), the resolution is better than at the high frequencies (small scales). Accordingly, the time resolution is better for high-frequency than it is for low-frequency components. In order for peaks to be detected at f_1 and f_2 ($f_1 > f_2$), they must be separated by at least one-half of the standard deviation of the peak at the higher frequency, thus requiring $f_1 - f_2 \geq f_1/4\pi f_0$. The choice of f_0 determines the current frequency resolution. By choosing $f_0 = 1$, we obtain a simple relation between scale and frequency, $f = 1/s$. Slow events are examined with a long window, while a shorter window is used for faster events. The Morlet wavelet provides optimal time-frequency localization within the limits imposed by the uncertainty principle.

2. Definition of the wavelet bispectrum

For the case of the wavelet bispectrum, the definitions are analogous to those used in Fourier-based bispectral analysis [16,17]. The wavelet bispectrum (WB) B_W is given by

$$B_W(s_1, s_2) = \int_T W_g(s_1, \tau) W_g(s_2, \tau) W_g^*(s, \tau) d\tau, \quad (13)$$

where

$$\frac{1}{s_1} + \frac{1}{s_2} = \frac{1}{s}. \quad (14)$$

The WB measures the amount of phase coupling in the interval T that occurs between wavelet components of scale lengths s_1, s_2 , and s of a signal $g(t)$, in such a way that the frequency sum rule (14) is satisfied. It is a complex quantity, defined by its magnitude A and phase ϕ :

$$B_W(s_1, s_2) = |B_W(s_1, s_2)| e^{j\angle B_W(s_1, s_2)} = A e^{j\phi}. \quad (15)$$

The instantaneous biphas calculated from (13) and (15) is

$$\phi(s_1, s_2, t) = \phi_{s_1}(t) + \phi_{s_2}(t) - \phi_s(t). \quad (16)$$

If two scale components s_1 and s_2 are scale and phase coupled, $\phi_s = \phi_{s_1} + \phi_{s_2}$, it holds that the biphas is 0 (2π) rad. For our purposes, the phase coupling is less strict because scale-dependent components can be phase delayed. We consider phase coupling to exist if the biphas is constant (but not necessarily 0 rad) for at least several periods of the highest scale component.

Simultaneously, we observe the instantaneous biamplitude, from which it is possible to infer the relative strength of the interaction

$$A(s_1, s_2, t) = |B_W(s_1, s_2, t)|. \quad (17)$$

Analogously to the case of the Fourier cross bispectrum, one can define a wavelet cross bispectrum as

$$B_{Wcfgg}(s_1, s_2) = \int_T W_f(s_1, \tau) W_g(s_2, \tau) W_g^*(s, \tau) d\tau. \quad (18)$$

For ease of interpretation, the WB is plotted in the (f_1, f_2) plane, rather than in the (s_1, s_2) plane. It possesses the same symmetries in the frequency domain as the Fourier-based

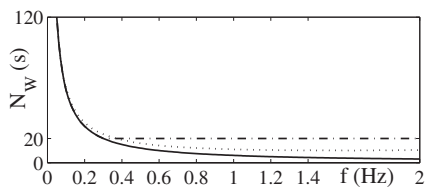


FIG. 1. Variation of the lengths N_W of Morlet-like wavelets with frequency (scale): Morlet wavelet (solid line); adapted Morlet wavelet (dotted line); and fixed wavelet length for high frequencies (dash-dotted line)

bispectrum (FB) B_F [27]. The nonredundant region of the WB is called its principal domain. The principal domain can be further divided into two triangular regions in which the WB has different properties [28]: the inner triangle (IT), and the outer one. Our interest centers on the IT [22,29].

3. Wavelet bispectrum adapted to real signals

The relationship between the frequency (scale) and the width of the window used for calculation of the wavelet transform is hyperbolic. A log-log scale is therefore a natural choice for its presentation. However, to be able to comply with the frequency (scale) sum rule (14), we need to achieve better frequency (scale) resolution for high frequencies (low scales) as can be effected by use of the Morlet wavelet when f_0 is chosen to be 1. Otherwise, nearby peaks at high frequencies cannot be resolved. For this purpose we introduce parameters d and a_m into the Morlet wavelet

$$\psi(u) = a_m c_n e^{-2\pi f_0 u e^{-u^2/d}}, \quad (19)$$

where the constant $c_n = 3.9487\pi^{-1/4}$. The parameter d determines the exponential decay of the Gaussian. This attenuates the Morlet wavelet, and thus permits the choice of a suitable combination of time and frequency (scale) resolution. The time resolution is $\Delta t = sd$, given by the decay of the exponential part of the wavelet. As d increases ($d > 1$), the frequency (scale) resolution improves, whereas the time resolution deteriorates; d is set such that the Gaussian function decays to 0.001 for each scale. A high value of d would cause a non-zero value of the Morlet window at its edges, resulting in side lobes on the WB. If d were infinite, the Morlet window would become a unit window, and the wavelet transform would become the selective discrete Fourier transform (SDFT) [31]. We wish to choose the frequencies in the analysis procedure freely, i.e., not restricted to $s \in \{2^n\}$, which implies a certain redundancy in the wavelet transform coefficients.

The frequency resolution at high frequencies is still insufficient: it is necessary to increase the length of the Morlet wavelet for high frequencies. This can be achieved in different ways. Figure 1 shows the hyperbolic decay of the Morlet wavelet length with increasing frequency (solid line). The wavelet length can be multiplied by a factor a_m , equal to that for the lowest frequency of interest, and then increased with increasing frequency,

$$a_m = 2^{1.8(f-f_{\min})/(f_{\max}-f_{\min})}, \quad (20)$$

where $f=1/s$ is the frequency of observation, and f_{\min} and f_{\max} define the frequency range of interest. The constant, 1.8, is set experimentally. In this way, we obtain the dotted line in Fig. 1. As the wavelet length is prolonged for high frequencies, the frequency resolution increases, whereas the time resolution deteriorates. Another way to obtain the necessary frequency resolution is to use a fixed wavelet length for all high frequencies, as shown by the dash-dotted line in Fig. 1.

WB estimation using the Morlet mother wavelet encounters a normalization problem. For each scale, a window of different length is used. In the case of a signal composed of different frequency components, but equal Fourier powers, this would result in different wavelet spectral energies for different frequencies. Two couplings among different frequencies with the same Fourier powers and the same nature of coupling, would result in different coupling strengths in the wavelet bispectrum. In (6), a factor $|s|^{-1/2}$ is used to ensure energy preservation. We choose to use a factor $1/N_W$ instead, where N_W is the Morlet window length. In this way, we can compare results obtained using FB and WB, since both preserve energy.

Normalization of the WB is achieved in the same way as for the FB [11]. The normalized WB indicates the average level of quadratic nonlinear phase coupling and, in a way, serves as an indicator of how non-Gaussian the signal is [32]. The critical values for the WB and biamplitude estimates were normalized to 1. If the estimated value is higher than the average value of WB in the IT, then it is taken as valid. By critical value, we mean that a value exceeds the noisy background (other than Gaussian), rounding, and estimation errors.

4. Instantaneous frequency

The bispectrum is sensitive to time variations of the frequency components, and it acquires a characteristic diagonal elongation of peaks. Bifrequencies where peaks in the bispectrum (wavelet) provide evidence of possible phase and/or frequency interactions are further studied by calculation of the biphase and biamplitude as functions of time. In doing so we do not follow time variations of the frequencies in the bifrequency pair when estimating time-biphase or -biamplitude dependence. They are estimated only for the peak bifrequency, i.e., where the average amplitude in the bispectrum takes its highest value. If the bifrequencies change considerably during the time of observation, such an approach can yield misleading results. It is of course possible to calculate the biphase and biamplitude for all the bifrequencies near the peak bifrequency and to plot them simultaneously in a graph, thus obtaining the time variations of the coupled frequency components and the evolution of the biphase and biamplitude. The interpretation, however, is rather difficult.

To be able to trace changes in the bifrequency (f_1, f_2) under study, we need to incorporate the instantaneous frequencies [33] $f_1(t)$ and $f_2(t)$ into the bispectral analysis. In this way we can calculate the instantaneous biphase and instantaneous biamplitude for the instantaneous bifrequency

$(f_1(t), f_2(t))$. Such an approach should lead to better results for the time dependence of the biphasic and biamplitude. There are two main methods to determine the instantaneous frequency of an oscillatory process, based on (i) marked events, and (ii) an analytic signal.

The marked events method involves marking events that indicate completion of one cycle of oscillation. The frequencies determined from sequential pairs of marked events are then linearly interpolated to obtain instantaneous values. Minimal or maximal values of the signal are usually taken as marked events. For instance, the R peak is strongly pronounced in an electroencephalogram (ECG) signal. It is easily distinguishable and can be automatically detected. The marked events approach can be applied easily in the case of signals where one oscillatory component dominates. However, not all processes in the blood distribution system can be measured selectively. Most of the quantities that can be measured, such as cardiovascular signals [24], contain multiple oscillatory processes and maxima and minima are no longer uniquely determined.

The second approach is based on the Hilbert transform [34]. From the signal under observation, $x(t)$, we construct an analytic signal

$$\zeta(t) = x(t) + ix^H(t) = A(t)e^{j\phi(t)}, \quad (21)$$

which is a complex function of time. The function $x^H(t)$ is the Hilbert transform of $x(t)$; $A(t)$ and $\phi(t)$ are, respectively, the instantaneous amplitude and phase. The instantaneous frequency $f(t)$ can be obtained by numerical differentiation of $\phi(t)$. In general, this may result in very large fluctuations in the estimate of $f(t)$ due to the influence of noise and/or the complicated form of the signal. Although $\phi(t)$ can be calculated formally for arbitrary $x(t)$, it has a clear physical meaning if $x(t)$ is a narrowband signal, in which case the instantaneous frequency corresponds to that of the maximum in the instantaneous spectrum. Several methods are available for estimation of $f(t)$ in the (usual) case where we are not interested in the behavior of a frequency on time scales smaller than its characteristic oscillation period [35].

We suggest a combination of both methods to obtain the instantaneous frequencies of oscillatory processes in the cardiovascular system, depending on the shape of the signal under scrutiny. The instantaneous frequency of cardiac oscillations is best calculated from ECG and blood pressure signals using the marked events method. Marked events can also be used to obtain the instantaneous frequency of the respiratory oscillations directly from the respiration signal, whereas the analytic signal procedure is best applied to calculate the instantaneous respiratory frequency from blood flow signals. In the latter case the signal must first be band-pass filtered in the frequency domain, by assigning zero values to all amplitudes outside the respiratory frequency range [30].

Note that the phase can also be obtained by direct use of the coefficients of the complex continuous wavelet transform [36], a method that has been shown to yield a precision comparable to that obtained by the marked events method and the Hilbert transform. The combination of the wavelet trans-

form and the bispectral analysis may further improve the precision of phase detection, as the phases obtained are continuous and the trade-off between frequency and time localization may further be optimized by taking account of the second-order statistics of the bispectra. However, this is a matter that needs additional investigation and will be reported elsewhere in due course.

III. ANALYSIS

A. Test signal

To illustrate the essence of the method, and to test it, we use a generic model of two interacting systems whose basic unit is the Poincaré oscillator

$$\begin{aligned} \dot{x}_1 &= -x_1q_1 - \omega_1y_1 + \eta_2(x_1 - x_2)^2 + \xi(t), \\ \dot{y}_1 &= -y_1q_1 + \omega_1x_1 + \eta_2(y_1 - y_2)^2, \\ \dot{x}_2 &= -x_2q_2 - \omega_2y_2, \\ \dot{y}_2 &= -y_2q_2 + \omega_2x_2, \\ q_i &= \alpha_i(\sqrt{x_i^2 + y_i^2} - a_i). \end{aligned} \quad (22)$$

The activity of each subsystem is described by the two state variables x_i and y_i , where $i=1,2$ denotes the subsystem, α_i , a_i and ω_i are constants, and η_2 is the coupling amplitude. The parameters of the model are set to $\alpha_1=1$, $a_1=0.5$, and $\alpha_2, a_2=1$. Here $\xi(t)$ is zero-mean white Gaussian noise $\langle \xi(t) \rangle = 0$, $\langle \xi(t), \xi(0) \rangle = D\delta(t)$, and $D=0.08$ is the noise intensity.

The test signal is the variable $x_{1A}(t)$ of the first oscillator, recorded as a continuous time series as shown in Fig. 2(a). Prior to analysis, the signal was first normalized between 0 and 1 and its mean value was subtracted. For the first 400 s, there was quadratic coupling with $\eta_2=0.2$. After a further 400 s, the forcing was removed by setting $\eta_2=0$. During the last 400 s, the coupling was increased again to $\eta_2=0.2$. In the latter case the characteristic frequency of the second oscillator was both modulated and linearly increased from $f_2=0.25$ to 0.35 Hz, as shown in Fig. 3(a). The first 15 s of each of the three coupling modes are shown in Fig. 2(a), with the corresponding power spectra in Fig. 2(b).

A standard fourth-order Runge-Kutta method (RK4) was used for the numerical integration. The initial values and step size were set to $x_1=-0.1$, $y_1=1.0$, $x_2=-0.1$, $y_2=1.0$, $h=0.01$. The signal x_1 was then resampled to 10 Hz.

B. Wavelet bispectrum

A quadratic nonlinear interaction between linear or weakly nonlinear oscillatory systems generates higher-harmonic components in addition to the characteristic frequencies [22,37]. Figure 2(b) illustrates the changes in the power spectra caused by the coupling. The peaks at $f_1=1.1$ Hz and $f_2=0.25$ Hz refer to the first and second oscillators, respectively. These frequencies are deliberately chosen to approximate an integer ratio 1:4 to ensure frequency

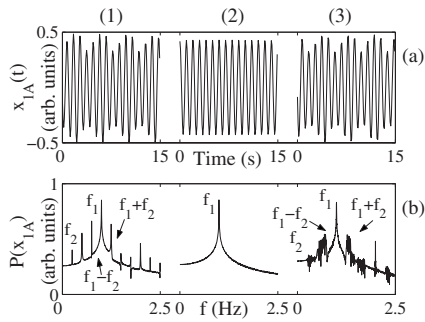


FIG. 2. Simulation results for a pair of quadratically coupled Poincaré oscillators in the presence of additive Gaussian noise. (a) The test signal $x_{1A}(t)$ from the first oscillator, after normalization and subtraction of its mean value. The first oscillator has a characteristic frequency $f_1=1.1$ Hz. That of the second oscillator is $f_2=0.25$ Hz. The oscillators are unidirectionally and quadratically coupled with three different coupling strengths: in column (1) $\eta_2=0.2$, (2) 0, and (3) 0.2. In column (3) the characteristic frequency of the second oscillator is linearly increased from $f_2=0.25$ to 0.35 while being at the same time modulated with $0.0013 \sin(2\pi 0.01t)$. Each coupling lasts for 400 s. The sampling frequency $f_s=10$ Hz. Only the first 15 s are shown in each case. (b) The corresponding power spectra of $x_{1A}(t)$.

coupling. The test signal x_{1A} clearly has richer harmonic structure in the presence of nonlinear coupling. In addition to the characteristic frequency of the first oscillator, it contains components with frequencies $2f_1$, $2f_2$, f_1+f_2 , and f_1-f_2 . As well as having a particular harmonic structure, the components of the signal x_{1A} also have related phases $2\phi_1$, $2\phi_2$, $\phi_1+\phi_2$, and $\phi_1-\phi_2$.

For bispectral analysis the whole signal is analyzed as a single entity, after the transients caused by the changes in coupling strength have been removed. First the WB is estimated, as shown in Figs. 4(a) and 4(b). Close inspection shows that all the peaks expected to arise from bispectral analysis of the nonlinear interaction between the two oscillators f_1 and f_2 are indeed present. Quadratic coupling has already been discussed in detail in [11] and is not a subject of this paper.

Bifrequencies where peaks provide evidence of possible frequency interactions are then further studied by calculation of the biphas and biamplitude as functions of time. Diagonal elongation of peaks in the bispectrum demonstrates time variation of the corresponding frequency components. The characteristic frequency of the second oscillator f_2 varies

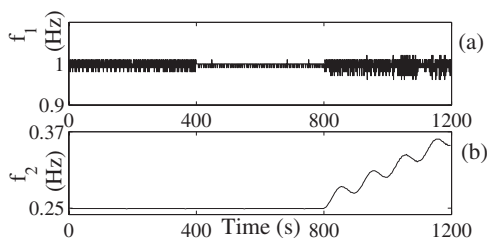


FIG. 3. Instantaneous frequencies of (a) the first oscillator f_1 and (b) the second oscillator f_2 , used for generating the test signal x_{1A} .

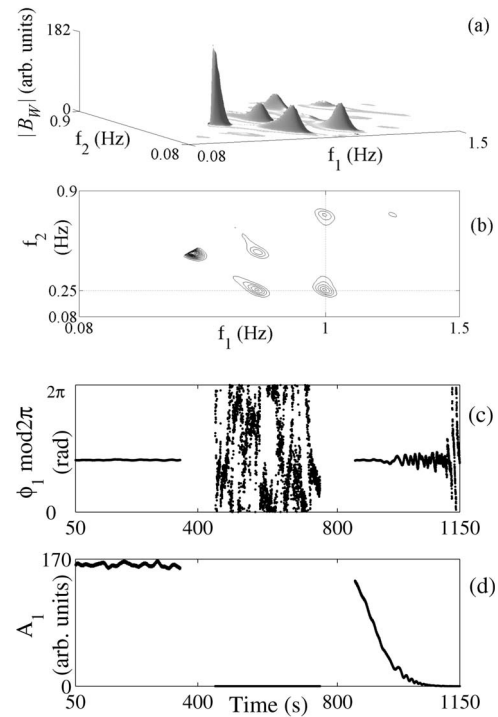


FIG. 4. (a) The modulus of the wavelet bispectrum $|B_W|$ calculated for $K=34$ segments, 67% overlapping, with $T_m=8$ s, $G_e=0.001$, using a fixed Morlet wavelet length of $T_{HF}=40$ s for calculation of the high frequencies. (b) A contour plot of the WB. Above $f_2>0.9$ Hz, the wavelet bispectrum is removed because the triplet (1.1 Hz, 1.1 Hz, 1.1 Hz) produces a high peak that is not physically significant. (c) The biphas ϕ_1 and (d) the biamplitude A_1 for the bifrequency (1 Hz, 0.25 Hz) peak 1, calculated using a 0.1 s time step. These calculations make no allowance for variations in instantaneous frequencies.

within 0.25–0.35 Hz. Our primary interest lies in the bifrequency (f_1, f_2) . The time evolution of its biphas and biamplitude are shown in Figs. 4(c) and 4(d). The results for nonzero coupling are quite different from those where coupling is absent (the second 400 s). The biphas is constant in the presence of quadratic coupling (first 400 s) and the biamplitude is above zero. Let us concentrate on the third 400 s, where one of the bifrequency components is varying. In the bispectrum we concentrate on the peaks where possible phase and/or frequency couplings are occurring. Here, we estimate the time evolution of the biphas for the peak bifrequency, i.e., where the average biamplitude takes its highest value. This is why, near 800 s where the characteristic frequency of the second oscillator f_2 has not risen much above 0.25 Hz, we obtain constant biphas and high biamplitude as shown in Figs. 4(c) and 4(d). As f_2 continues to grow linearly (but with modulation) to 0.35 Hz, the biamplitude drops toward zero and the biphas exhibits phase slips, falsely suggesting that there is no coupling.

C. Instantaneous frequency

Figures 5(a) and 5(b) show the biphas and biamplitude, taking explicit account of the instantaneous bifrequency. In

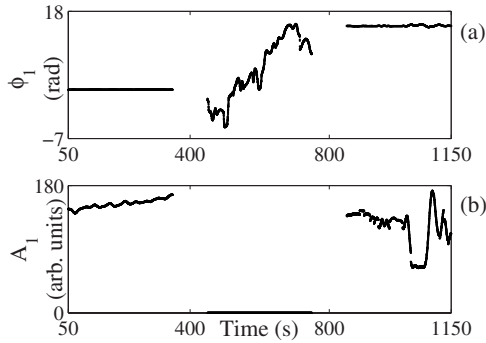


FIG. 5. Wavelet bispectral estimates based on the instantaneous frequencies $f_1(t)$ and $f_2(t)$, which were obtained using the marked events method. (a) The instantaneous biphasse ϕ_1 and (b) the instantaneous biamplitude A_1 for the bifrequency (1.1 Hz, 0.25 Hz) peak 1, calculated for $K=34$ segments, 67% overlapping, with $T_m=8$ s, $G_e=0.001$, using a fixed Morlet wavelet length of $T_{HF}=40$ s for the calculation of high frequencies and a 0.1 s time step.

doing so, the instantaneous frequencies $f_1(t)$ and $f_2(t)$ [Figs. 3(a) and 3(b)] were both obtained using the marked events method. The results for nonzero coupling are quite different from those where coupling is absent (second 400 s). The biphasse is constant in the presence of quadratic coupling (first 400 s) and the biamplitude takes a finite value. During the final 400 s, when there is a large time-frequency variation of the second oscillator's frequency, the biamplitude is again above zero and the biphasse remains constant during the whole time of observation—both features being clearly resolved despite the nonlinear coupling. Bispectral analysis was also performed using instantaneous frequencies $f_1(t)$ and $f_2(t)$, where both of them were obtained directly from Eq. (22). The results were exactly the same.

IV. COMPARISON OF FOURIER- AND WAVELET-BASED BISPECTRA

We now present some simulation results to illustrate the main reason for sometimes preferring to use wavelet-based rather than Fourier-based bispectra. We then discuss the main strengths and weaknesses of the two methods.

We again use the same generic model, Eq. (22) with quadratic coupling, now taking $f_1=1.1$ Hz and $f_2=0.24$ Hz. The model parameters α_i , a_i , and D are the same as for the test signal x_{1A} [Fig. 2(a)]. In this way, we obtain the test signal $x_{1B}(t)$ shown in Fig. 6(a) from the first oscillator, recorded as a continuous time series. The two coupling strengths of $\eta_2=0$ (no coupling) and $\eta_2=0.2$ (weak coupling) are interchanging every 20 s. Only the first 15 s of $x_{1B}(t)$ are shown for each coupling mode. The corresponding power spectra are shown on Fig. 6(b).

Figures 7(a) and 7(b) show the FB in perspective and contour plots, respectively, for the test signal x_{1B} . We concentrate on the bifrequency of primary interest, $f_1(t)$, $f_2(t)$. In the first case a 100 s window was used for estimating DFTs. Details of how to choose the window length are given in [37]. The calculated instantaneous biamplitude and biphasse

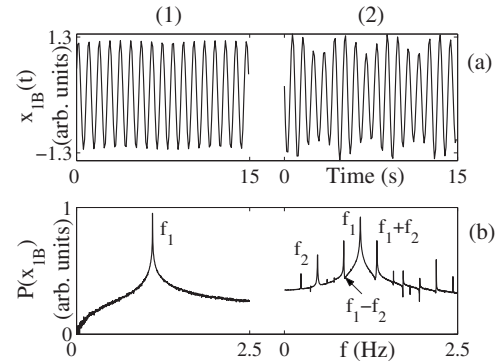


FIG. 6. Simulation results for time-intermittent quadratic couplings in the presence of additive Gaussian noise. (a) The test signal $x_{1B}(t)$ from the first oscillator, with characteristic frequency $f_1=1.1$ Hz. The characteristic frequency of the second oscillator was $f_2=0.24$ Hz. The oscillators are unidirectionally and quadratically coupled with two different coupling strengths: column (1) $\eta_2=0$; and (2) $\eta_2=0.2$. The coupling in column (2) is present every 20 s and lasts for 20 s. The signal is 1200 s long and sampled with sampling frequency $f_s=10$ Hz. Only the first 15 s are shown in each case. (b) The corresponding power spectrum of $x_{1B}(t)$.

are presented in Figs. 7(c) and 7(d). The biphasse increases monotonically and there are no episodes of constant biphasse, although the biamplitude remains high during the whole time of observation.

In a second set of calculations, a 130 s window was used for estimating DFTs. The corresponding biamplitude and biphasse are shown in Figs. 7(e) and 7(f). The biphasse tends to be constant (remains within a $\pi/2$ range) and the biamplitude is high (more than twice the average value of the FB within the inner triangle).

It is evident that, for the detection of short episodes ($< \frac{1}{2}$ the DFT window length) of nonlinear coupling, the FT method is not appropriate. It can lead to misleading interpretation of the bispectral estimates, either of no coupling in the first case or of quadratic coupling in the second case.

Figures 8(a) and 8(b) show the WB in perspective and contour views, respectively, for the same signal x_{1B} . The wavelet-based method clearly gives the same information about the peak's relative amplitude and bifrequency as the Fourier-based method, but the frequency resolution is evidently lower than in the latter case. The calculated instantaneous biamplitude and biphasse are presented in Figs. 8(c) and 8(d) respectively. They clearly reveal the intervals during which the coupling is present or absent. By increasing the time resolution for calculation of the WB at high frequencies, we obtain precisely the times at which the intermittent quadratic coupling occurs, i.e., every 20 s, Fig. 8(e) and 8(f).

A. Overview of main advantages and weaknesses of Fourier and wavelet bispectra

We now overview the relative strengths and weaknesses of the Fourier-based and wavelet-based methods of calculating bispectra. There are several points to consider.

(1) *Time and frequency resolution.* To observe a given

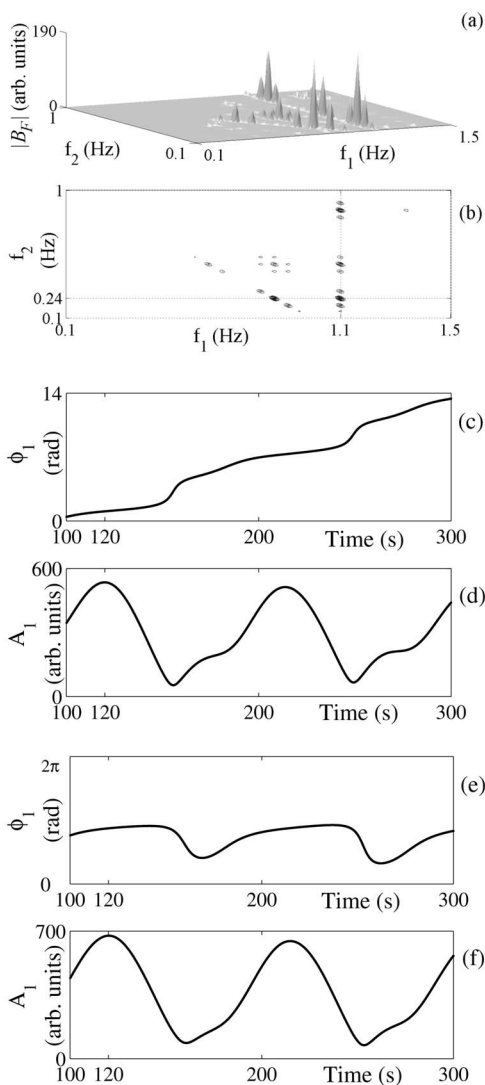


FIG. 7. Analyses of the test signal with time-intermittent quadratic couplings, in the presence of additive Gaussian noise using the Fourier-based bispectral method. (a) The Fourier-based bispectrum $|B_F|$ for signal x_{1B} calculated with $K=33$ segments, 66% overlapping and using the Blackman window to reduce leakage and (b) its contour view. The part of the bispectrum above $f_2 > 1.0$ Hz has been cut because the triplet (1.1 Hz, 1.1 Hz, 1.1 Hz) produces a high peak that is physically meaningless. (c) The biphase ϕ_1 . (d) The biamplitude A_1 for the bifrequency (1.1 Hz, 0.24 Hz), calculated with a 100-s-long window for estimating DFTs. (e) The biphase and (f) the biamplitude calculated with a 130 s window for estimating DFTs. In both cases, a 0.3 s time step was used and the Blackman window was applied.

frequency, the signal must be observed over at least one period of this frequency, which inevitably limits time localization. Due to the uncertainty principle [21], sharp localization in time and frequency are of course mutually exclusive:

$$\Delta t \Delta f = \frac{1}{4\pi}, \quad (23)$$

where t is the time interval and f is the frequency band. The equality holds if and only if the window is Gaussian.

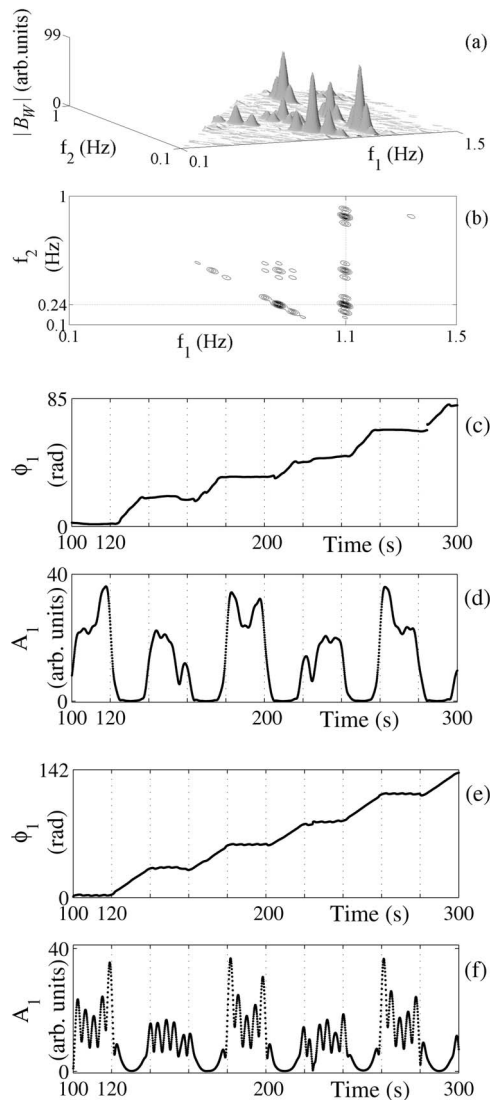


FIG. 8. Analyses of a test signal for time-intermittent quadratic couplings in the presence of additive Gaussian noise using the wavelet bispectral method. (a) The wavelet bispectrum $|B_W|$ calculated with $K=33$ segments and 66% overlapping. The part of the bispectrum above $f_2 > 1.0$ Hz is removed, because the triplet (1.1 Hz, 1.1 Hz, 1.1 Hz) produces a high peak that is physically meaningless. (c) The biphase ϕ and (d) biamplitude A_1 for bifrequency (1.1 Hz, 0.24 Hz), calculated with $G_e=0.01$. (e) The biphase ϕ and (f) biamplitude A_1 , calculated with $G_e=0.0001$. In both cases, the time step was 0.1 s, $T_m=8$ s, and a $T_{HF}=20$ s fixed Morlet wavelet length was used for estimating high frequencies.

In general, the WB detects intermittent phase couplings well, whereas the FB averages out most of the time-relevant information. The triplet (f_1, f_2, f_3) results in a high peak in the bispectrum if the coupling condition $f_3 = f_1 + f_2$, is satisfied (within the frequency resolution). Because the frequency resolution changes with frequency, this condition is less strict for WB analysis. If there is a mismatch in the coupling frequency f such that $f_3 = f_1 + f_2 + \Delta f$, where Δf is larger than the frequency resolution of the FB but smaller than the WB frequency resolution, then the WB will peak for the triplet (f_1, f_2, f_3) , whereas the FB will not. By increasing the fre-

quency resolution of the WB (increasing the length of the Morlet wavelet for high frequencies) we obtain approximate results, as can also be obtained with the FB.

On the other hand, if there is a brief episode of coupling between the oscillators, the FB-based method cannot detect it from the signal due to the large time window used, whereas the WB will detect it, down to a certain minimum duration. Thus the WB allows intermittent couplings to be detected. When applying the FB to real data, we have to ensure the necessary frequency resolution to be able to distinguish separate frequency components and at the same time achieve sufficient time resolution to be able to detect the onset of couplings among the cardiovascular oscillators. The scope for choice of window length is limited by the uncertainty principle [21], and compromise is inevitably needed between time and frequency resolution.

In contrast to the FB, the WB based on Morlet's mother wavelet enables us to enjoy optimal time and frequency resolution at the same time, which is an obvious advantage compared to the FB.

Since the time resolution of the WB is higher at high frequencies compared to the FB, and the frequency resolution poorer, it is necessary to ensure that there is sufficient frequency resolution before attempting to interpret the results obtained. Poor frequency resolution would obviously result in poor or incorrect localization of the characteristic frequencies. Excessively high time resolution could result in a too-high sensitivity to noise and statistical error, in turn resulting in phase slips and incorrect detection of the onset and duration of the interoscillator coupling. For our purposes, the time and frequency resolution was set in such a manner that coupling episodes of approximately ten periods of the lower frequency are detectable (to overcome coincidence couplings), and the characteristic frequencies can still be estimated to better than 10% [37].

(2) *Frequency step.* Once the window length is chosen, the frequency resolution is set and fixed for the FB. This is not the case when using the wavelet transform. Since the wavelet transform is continuous, the frequency step can be arbitrarily chosen. In this way, the transform can be over-sampled in time for large scales, and we are not concerned about the inverse transform.

(3) *Energy preservation.* Cardiovascular signals, which provided the main motivation for this study, are signals whose power is of interest [23]. The FB is based on the DFT, which gives the signal's energy (power) directly. In the case of the WB, normalization is necessary to obtain the signal's energy (power).

(4) *Statistical error.* Integration over finite time series in order to calculate the WB results in an additional noise contribution. It is called the statistical noise level since it is the value of WB that would be computed for a white noise input signal, and is caused by the finite statistics (i.e., use of a limited number of values in the integrating or averaging process). In addition, there is also an error equal to the product of uncertainties in the determination of the individual wavelet bispectrum coefficients [16,21,22].

To calculate the WB, Eq. (13), the wavelet coefficients are determined for each of the $N_w = T f_s$ samples in the interval $T: \{T_0 - T/2 \leq \tau \leq T_0 + T/2\}$, and averaged, Eq. (7). If we as-

sume that all the estimates of the WB are independent, the averaged WB will suffer a statistical error of $1/\sqrt{N_w}$ due to summation over N_w values. Similarly, in the FB case the summation is carried out over N/M ensembles, where M is the number of points in each statistically independent ensemble for which an M -point DFT is calculated. The statistical error in the FB decays as $\sqrt{M/N}$, and a factor of M more points is needed to obtain the same statistical error as with the WB. From this point of view, the WB represents a significant improvement in the time resolution of the bispectrum. Although the wavelet coefficients are not all statistically independent, because the chosen wavelet family is not orthogonal, the statistical error is not twice as large [16]. This implies that WB analysis is able to detect coherent signals in extremely noisy data, provided that the coherence remains constant over sufficiently long intervals, because the noise contribution falls off rapidly with increasing N .

(5) *Bispectrum interpretation.* By choosing $f_0=1$ in Eq. (9) a simple relation between scale and frequency can be obtained, $f=1/s$. In this case the interpretation of the WB is the same as for the FB; otherwise it is not straightforward.

(6) *Computation.* The default WB window length decreases hyperbolically with increased frequency, whereas the FB uses a fixed window length. The WB is therefore computationally less demanding and much faster (and the same argument applies for the fast Fourier transform as compared to the fast wavelet transform). Moreover, relatively short data sequences are sufficient to perform a WB analysis, in contrast to the FB, which needs long time series to obtain both sufficient frequency resolution and adequate statistics.

B. Other possible methods for bispectrum estimation

The selective discrete Fourier transform (SDFT), a hybrid of the Fourier and wavelet transforms, can also be used for calculation of the bispectrum. The modified STFT was first introduced by Keselbrener and Akselrod [31]. Like the STFT it is a time-dependent Fourier transform. The required time-frequency sensitivity is obtained by applying a different window of appropriate length for estimation of each spectral component. Low frequencies are expected to vary slowly, whereas high frequencies are expected to vary rapidly, i.e., undergo sudden changes. For each frequency of interest, a DFT calculation is performed, while the time window around the considered data point is made of length inversely proportional to the frequency of interest. This is actually similar to the wavelet transform's stretching and compressing of the mother wavelet. Therefore narrow windows are used for estimating high frequencies and wide ones for low frequencies, implying that low frequencies are estimated with good frequency resolution and high frequencies with good time resolution.

For each time scale of interest, spectral components are calculated using different lengths of window, $T=N_p/f$. The parameter N_p , $N_p \in \mathbb{Z}$, is the number of entire periods within the window. A high value of N_p will lead to poor time resolution (wide window), whereas a small value will lead to a less reliable estimate of the spectral components in the case of noisy signals. The value needed to produce optimal results

is determined experimentally and usually lies in the range 4–8.

Leakage may appear in the spectrum if the signal entering the rectangular window is not periodic or, at least, if the amplitudes of the end points are unequal. In order to remove such leakage, the data are usually convolved with some kind of smoothing window, such as a Hamming, Hanning, or Blackman window. Their role is to taper the windowed data in order to make the two end point amplitudes smoothly equal. Besides the leakage removal, these tapering windows also improve the time resolution of the time-dependent spectral analysis.

The SDFT and WT provide similar results. Both transforms use a specific window length to estimate each spectral component. The SDFT uses convolution with a Blackman, Hanning, Hamming, or other taper window whereas the WT uses different mother wavelets such as the Morlet. Both methods allow choice between good time or good frequency resolution. We can change frequency and time resolution by changing parameters, but we cannot increase them both simultaneously because of the uncertainty principle. The WT obtained with the Morlet wavelet provides optimal time-frequency resolution; while when using the SDFT this optimum can also be approached by an appropriate choice of parameters. They can both be normalized to energy. The main difference between the transforms is that the WT is continuous whereas the SDFT is not. Note that the frequency (scale) sum rule (14) is much easier to comply with if a continuous transform is used.

V. SUMMARY AND CONCLUSIONS

We have introduced wavelet-based bispectral analysis using the Morlet mother wavelet, allowing for a clear scale-to-frequency relationship. Since the time resolution of the wavelet bispectrum is higher and the frequency resolution

poorer at high frequencies compared to the Fourier-based bispectrum, it is necessary to ensure sufficient frequency resolution to preserve the scale (frequency) sum condition by increasing the length of the Morlet wavelet for high frequencies. When the characteristic frequencies vary in time over a significant frequency interval the bifrequency (f_1, f_2) also has to be time sensitive, and we therefore introduced the instantaneous bifrequency $(f_1(t), f_2(t))$ into the wavelet bispectral analysis.

The advantages of wavelet- over Fourier-based bispectral analysis are significant. Using the wavelet bispectrum, intermittent phase couplings can be detected, whereas the Fourier bispectrum averages out most of the time-relevant information. The WB allows an arbitrary frequency step to be chosen, thus ensuring optimal time and frequency resolution. There is a simple relationship between scale and frequency; it has a smaller statistical error and is computationally less demanding than for the FB. The only drawbacks are that it has to be normalized to obtain signal energy and is nonorthogonal. However normalization can be performed since we are not concerned with the inverse wavelet transform.

In general, the proposed wavelet bispectral analysis provides a promising tool for studying the type of coupling between two or more nonlinear oscillators whose basic frequencies change considerably in time. We conclude that wavelet-based bispectral analysis has potential for useful application to complex interacting systems that yield multivariate time series. The method enables several aspects of the interaction to be characterized simultaneously.

ACKNOWLEDGMENTS

The study was supported by the Royal Society, Slovenian Research Agency, Wellcome Trust (U.K.), and the EU NEST Path-finder Tackling Complexity in Science project BRACCIA.

-
- [1] S. H. Strogatz, D. M. Abrams, A. McRobie, B. Eckhardt, and E. Ott, *Nature (London)* **438**, 43 (2005).
 - [2] S. Nakamura, *J. Construct. Steel Res.* **62**, 1148 (2006).
 - [3] G. B. Ermintrout and J. Rinzel, *Am. J. Physiol.* **246**, R102 (1984).
 - [4] C. Schäfer, M. G. Rosenblum, J. Kurths, and H.-H. Abel, *Nature (London)* **392**, 239 (1998).
 - [5] A. Stefanovska and M. Bračič, *Contemp. Phys.* **40**, 31 (1999).
 - [6] M. Hirota, T. Tatsuno, and Z. Yoshida, *Phys. Plasmas* **12**(1), 012107 (2005); T. Fukuyama, R. Kozakov, H. Testrich, and C. Wilke, *Phys. Rev. Lett.* **96**, 024101 (2006).
 - [7] D. DeShazer, R. Breban, E. Ott, and R. Roy, *Int. J. Bifurcation Chaos Appl. Sci. Eng.* **14**, 3205 (2004); W.S. Lam, P.N. Guzdar, and R. Roy, *Phys. Rev. E* **67**, 025604(R) (2003).
 - [8] R. Breban and E. Ott, *Phys. Rev. E* **65**, 056219 (2002); J. G. Restrepo, E. Ott, and B. R. Hunt, *ibid.* **71**, 036151 (2005).
 - [9] A. S. Pikovsky, M. G. Rosenblum, and J. Kurths, *Synchronization: A Universal Concept in Nonlinear Sciences* (Cambridge University Press, Cambridge, U.K., 2001).
 - [10] T. Schreiber, *Phys. Rev. Lett.* **85**, 461 (2000); M. G. Rosenblum and A. S. Pikovsky, *Phys. Rev. E* **64**, 045202(R) (2001); M. G. Rosenblum, L. Cimponeriu, A. Bezerianos, A. Patzak, and R. Mrowka, *ibid.* **65**, 041909 (2002); M. Paluš, V. Kormárek, Z. Hrnčič, and K. Štěrbová, *ibid.* **63**, 046211 (2001); M. Paluš and A. Stefanovska, *ibid.* **67**, 055201(R) (2003).
 - [11] J. Jamšek, A. Stefanovska, P. V. E. McClintock, and I. A. Khovanov, *Phys. Rev. E* **68**, 016201 (2003); J. Jamšek, M.S. thesis, University of Ljubljana, 2000 (unpublished).
 - [12] M. B. Priestley and M. M. Gabr, *Multivariate Analysis: Future Directions* (North-Holland, Amsterdam, 1993).
 - [13] J. R. Fonoliosa and C. L. Nikias, *IEEE Trans. Signal Process.* **41**, 245 (1993); B. Boashash and P. J. O'Shera, *ibid.* **42**, 216 (1994); T. S. Rao and K. C. Indukumar, *J. Franklin Inst.* **333**, 425 (1996); R. J. Perry and M. G. Amin, *IEEE Trans. Signal Process.* **43**, 1017 (1995); A. V. Dandawaté and G. B. Giannakis, *IEEE Trans. Inf. Theory* **41**, 216 (1995).
 - [14] A. Swami, G. B. Giannakis, and G. Zhou, *Signal Process.* **60**, 65 (1997).

- [15] B. Schack *et al.*, Clin. Neurophysiol. **112**, 1388 (2001).
- [16] B. Ph. van Milligen, C. Hidalgo, and E. Sánchez, Phys. Rev. Lett. **74**, 395 (1995); B. Ph. van Milligen, *et al.*, Phys. Plasmas **2**, 3017 (1995).
- [17] A. K. Nadi, *Higher-Order Statistics in Signal Processing* (Cambridge University Press, Cambridge, U.K., 1998).
- [18] V. K. Madiseti and D. B. Williams, *The Digital Signal Processing Handbook* (CRC Press, Boca Raton, FL, 1998).
- [19] R. Malek-Madani, *Advanced Engineering Mathematics* (Addison Wesley/Longman, Reading, MA, 1998).
- [20] V. DeBrunner, M. Özyaydin, and T. Przebinda, IEEE Trans. Signal Process. **47**, 783 (1999).
- [21] G. Kaiser, *A Friendly Guide to Wavelets* (Birkhäuser, Boston, 1994).
- [22] C. L. Nikias and A. P. Petropulu, *Higher-Order Spectra Analysis: A Nonlinear Signal Processing Framework* (Prentice-Hall, Englewood Cliffs, NJ, 1993).
- [23] J. G. Proakis and D. G. Manolakis, *Digital Signal Processing* (Prentice-Hall, Englewood Cliffs, NJ, 1996).
- [24] M. Bračič and A. Stefanovska, Bull. Math. Biol. **60**, 919 (1998); M. Bračič Lotrič, Ph.D. thesis, University of Ljubljana, 1999; A. Stefanovska, M. Bračič, and H. D. Kvernmo, IEEE Trans. Biomed. Eng. **46**, 1230 (1999); V. Urbančič-Rovan, B. Meglič, A. Stefanovska, A. Bernjak, K. Ažman-Juvan, and A. Kocijančič, Diabetic Med. **24**, 18 (2007); B. Musizza, A. Stefanovska, P. V. E. McClintock, M. Paluš, J. Petrovčič, S. Ribarič, and F. F. Bajrović, J. Physiol. **580**, 315 (2007).
- [25] A. Grossmann and J. Morlet, SIAM J. Math. Anal. **15**, 723 (1984).
- [26] I. Daubechies, *Ten Lectures on Wavelets* (SIAM, Philadelphia, 1992).
- [27] L. A. Pflug, G. E. Ioup, and J. W. Ioup, J. Acoust. Soc. Am. **94**, 2159 (1993); **95**, 2762 (1994).
- [28] M. J. Hinich, IEEE Trans. Acoust., Speech, Signal Process. **38**, 1277 (1990); I. Sharfer and H. Messer, IEEE Trans. Signal Process. **41**, 296 (1993); M. J. Hinich, *ibid.* **43**, 2130 (1995).
- [29] J. W. A. Fackrell, Ph.D. thesis, University of Edinburgh, 1996.
- [30] A. Stefanovska and M. Bračič, Control Eng. Pract. **7**, 161 (1999).
- [31] L. Keselbrenner and S. Akselrod, IEEE Trans. Biomed. Eng. **43**, 789 (1996).
- [32] M. J. Hinch, J. Time Ser. Anal. **3**, 169 (1982).
- [33] A. S. Pikovsky, M. G. Rosenblum, and J. Kurths, Europhys. Lett. **34**, 165 (1996); M. G. Rosenblum, A. S. Pikovsky, and J. Kurths, Phys. Rev. Lett. **76**, 1804 (1996); A. S. Pikovsky, M. G. Rosenblum, G. V. Osipov, and J. Kurths, Physica D **104**, 219 (1997); M. Entwistle, A. Bandvivyky, B. Musizza, A. Stefanovska, P. V. E. McClintock, and A. Smith, Br. J. Anaesth. **93**, 608P (2004).
- [34] D. Gabor, J. IEE London **93**, 429 (1946); P. Panter, *Modulation, Noise and Spectral Analysis* (McGraw-Hill, New York, 1965).
- [35] B. Boashash, Proc. IEEE **80**, 520 (1992); R. Quian Quiroga, A. Kraskov, T. Kreuz, and P. Grassberger, Phys. Rev. E **65**, 041903 (2002).
- [36] M. Palus, D. Novotna, and P. Tichavsky, Geophys. Res. Lett. **32**, L12805 (2005); M. Palus and D. Novotna, Nonlinear Processes Geophys. **13**, 287 (2006).
- [37] J. Jamšek, A. Stefanovska, and P. V. E. McClintock, Phys. Med. Biol. **49**, 4407 (2004).